Journal of Structural Chemistry. Vol. 56, No. 7, pp. 1342-1352, 2015.

SPECTROSCOPIC CHARACTERIZATION, X-RAY STRUCTURE AND DFT STUDIES ON 4-[3-(2,5-DIMETHYLPHENYL)-3-METHYLCYCLOBUTYL]-N-METHYLTHIAZOL-2-AMINE

H. Saraçoğlu[1] and Ö. Ekici[2]

UDC 548.73:547.53

The titled molecule 4-[3-(2,5-dimethylphenyl)-3-methylcyclobutyl]-N-methylthiazol-2-amine ($C_{17}H_{22}N_2S$) is synthesized and characterized by ^{1}H NMR, ^{13}C NMR, IR, and X-ray single crystal determination. The compound crystallizes in the monoclinic space group $P2_1/c$ with $a = 6.3972(4)$ Å, $b = 9.4988(6)$ Å, $c = 26.016(2)$ Å and $\beta = 93.496(7)°$. In addition to the molecular geometry from the X-ray determination, vibrational frequencies and gauge, including the atomic orbital (GIAO), ^{1}H and ^{13}C NMR chemical shift values of the titled compound in the ground state are calculated using the density functional (B3LYP) method with 6-31G(*d*), 6-31++G(*d*,*p*) and 6-311+G(2*d*,*p*) basis sets. The calculated results show that the optimized geometries can well reproduce the crystal structure. Moreover, the theoretical vibrational frequencies and chemical shift values show good agreement with the experimental values. The predicted nonlinear optical properties of the titled compound are greater than those of urea. DFT calculations of the molecular electrostatic potentials and frontier molecular orbitals of the titled compound are carried out at the B3LYP/6-31G(*d*) level of theory.

DOI: 10.1134/S002247661507015X

Keywords: synthesis, thiazole, computational chemistry, X-ray structure determination, NMR spectroscopy, nonlinear optical properties.

Various thiazole derivatives show herbicidal, anti-inflammatory, antimicrobial and antiparasite activity [1, 2] and also liquid crystal properties [3]. The thiazole ring is known to be a part of vitamin B1, cocarboxylase, and the cyclic system of penicillin [4]. Thiazole itself and its derivatives are of importance in biological systems as anti-inflammatory, analgesic agents and inhibitors on lipoxygenase activities [5, 6]. The most recognized structures of the starting substances and the titled compound are given in Scheme 1.

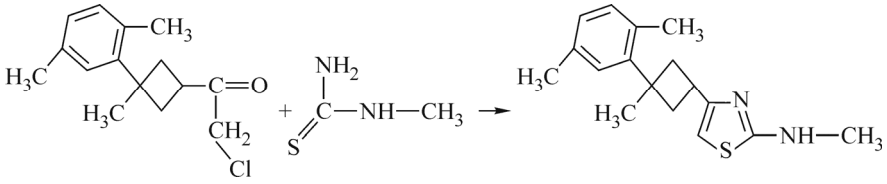

Scheme 1. Synthetic route for the synthesis of the target compound.

[1]Department of Middle Education, Educational Faculty, Ondokuz Mayis University, Kurupelit, Samsun, Turkey; hanifesa@omu.edu.tr, hanifesaracoglu@yahoo.com. [2]Department of Chemistry, Faculty of Sciences, Firat University, Elazig, Turkey. The text was submitted by the authors in English. *Zhurnal Strukturnoi Khimii*, Vol. 56, No. 7, pp. 1405-1414, November-December, 2015. Original article submitted January 27, 2015; revised March 26, 2015.

These ligands containing cyclobutane and thiazole in their molecules seem to be suitable candidates for further chemical modifications and may be pharmacologically active and useful as ligands in coordination chemistry. Taking into account the above observations, this compound has been synthesized in a similar manner of our ongoing research program for biologically active compounds [7].

In recent years, density functional theory (DFT) has been a shooting star in theoretical modeling. The development of ever better exchange-correlation functionals has made it possible to calculate many molecular properties with accuracies comparable with those of traditional correlated *ab initio* methods, with more favorable computational costs [8]. Literature surveys have revealed the high degree of accuracy of DFT methods in reproducing the experimental values in terms of geometry, dipole moment, vibrational frequency, and so on [9-15].

In this study, we present the results of a detailed investigation of the synthesis and structural characterization of 4-[3-(2,5-dimethylphenyl)-3-methylcyclobutyl]-N-methylthiazol-2-amine by single crystal X-ray diffraction, ^{1}H and ^{13}C NMR spectroscopy, and quantum chemical methods. The vibrational assignments of the titled compound in the ground state have been calculated using the DFT(B3LYP) method with 6-31G(*d*) and 6-31++G(*d*,*p*) basis sets. The structural geometry, molecular electrostatic potential (MEP), frontier molecular orbitals (FMO), and nonlinear optical properties of the titled compound were investigated. We also make comparisons between the experiment and the calculation.

EXPERIMENTAL

Synthesis of the titled compound. To a solution of 0.0902 g of 1-methylthiourea (1 mmol) dissolved in 50 ml of absolute ethanol, a solution of 0.251 g (1 mmol) of 2-chloro-1-[3-(2,5-dimethylphenyl)-3-methylcyclobutyl]ethanone, which was synthesized and purified according to the literature procedure [16], was added dropwise in 1-h period. After the addition of α-haloketone, the temperature was raised to 50-55°C and kept at this temperature for 2 h. The solution was cooled to room temperature and then made alkaline with an aqueous solution of NH_3 (5%), and yellow precipitate was separated by suction, washed with aqueous NH_3 solution several times and dried in air. Suitable single crystals for the crystal structure determination were obtained by slow evaporation of its ethanol solution. Light yellow crystals. Yield: 92%. M.p.: 190°C (EtOH).

Crystal structure determination. The data collection was performed at 296 K on a Stoe-IPDS-2 diffractometer equipped with graphite monochromated MoK_α radiation (λ = 0.71073 Å). The structure was solved by direct methods using SHELXS-97 and refined by a full-matrix least-squares procedure using the SHELXL-97 program [17]. All non-hydrogen atoms were easily found from the different Fourier maps and refined anisotropically. All hydrogen atoms were included using a riding model and refined isotropically with CH = 0.93 (for the phenyl group), CH_2 = 0.97, CH_3 = 0.96, CH = 0.98, and NH = 0.86 Å. U_{iso}(H) = 1.2U_{eq} (1.5 U_{eq} for the methyl group). Details of the data collection conditions and parameters of the refinement process: $C_{17}H_{22}N_2S$, M = 287.43, monoclinic, space group $P2_1/c$, a = 6.3972(4), b = 9.4988(6), c = 26.016(2) Å, β = 93.496(7)°, V = 1577.94(19) Å^3, Z = 4, d_c = 1.210 g/cm^3, μ = 0.198 mm^{-1}, F(000) = 620, crystal size 0.350×0.227×0.186 mm, θ range 3.18-28.98°, index ranges $-8 \le h \le 8$, $-5 \le k \le 12$, $-34 \le l \le 34$, 6838 reflections collected, 3577 independent (R_{int} = 0.062), 1341 observed ($I > 2\sigma(I)$), 182 parameters, final ($I > 2\sigma(I)$) R = 0.076, wR = 0.116, $GOOF$ = 1.00, Δρ = 0.19, Δρ = –0.20 e/Å^3.

Theoretical methods. DFT calculations with a hybrid B3LYP functional (Becke′s three-parameter hybrid functional using the LYP correlation functional) with 6-31G(*d*), 6-31++G(*d*,*p*), and 6-311+G(2*d*,*p*) basis sets were performed by the Berny method [18, 19] using the Gaussian 03 software package [20] and the Gauss-view visualization program [21]. The calculated and scaled by 0.9772 [22], 0.9537 [23] vibrational frequencies ascertained that the structures were stable (no imaginary frequencies).

The geometry of the titled compound, together with that of tetramethylsilane (TMS), was fully optimized. ^{1}H and ^{13}C NMR chemical shifts were calculated within the GIAO approach [24, 25] applying B3LYP with 6-31G(*d*) and 6-311+G(2*d*,*p*) basis sets.

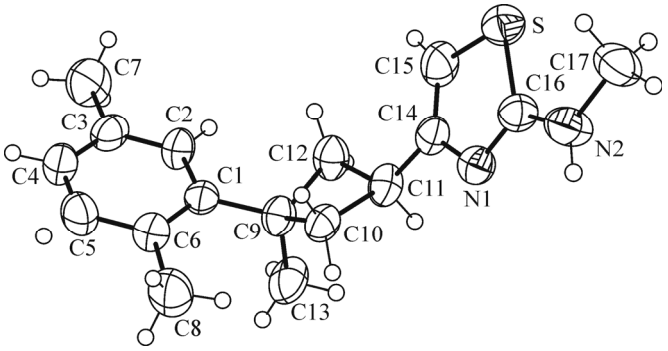

Fig. 1. ORTEP III diagram of the titled compound. Displacement ellipsoids are drawn at the 30 % probability level and H atoms are shown as small spheres of arbitrary radii.

To investigate the reactive sites of the titled compound the molecular electrostatic potential (MEP) was evaluated using the B3LYP/6-31G(*d*) method. MEP,*V*(*r*), at a given point *r*(*x*, *y*, *z*) in the vicinity of the molecule is defined in terms of the interaction energy between the electrical charge generated by the molecule electrons and nuclei and a positive test charge (a proton) located at *r*. For the system studied the *V*(*r*) values were calculated as described previously using the equation [26]

$$V(r) = \sum(Z_A / | R_A - r |) - \int(\rho(r') / | r' - r |)d^3r' , \quad (1)$$

where Z_A is the charge of nucleus A located at R_A, $\rho(r')$ is the electron density function of the molecule, and r' is the dummy integration variable. The linear polarizability and first hyperpolarizability properties of the titled compound were obtained by molecular polarizabilities based on theoretical calculations. In addition, the frontier molecular orbital (FMO) analysis was carried out at the same level.

RESULTS AND DISCUSSION

Description of the crystal structure. The titled compound, an ORTEP [27] view of which is shown in Fig. 1, crystallizes in the monoclinic space group $P2_1/c$ with four molecules in the unit cell. The asymmetric unit in the crystal structure contains only one molecule.

The titled compound contains thiazole, dimethylphenyl, and cylobutane moieties. The thiazole and phenyl rings are planar with maximum deviations of 0.0057(28) and –0.0036(22) Å, respectively. The dihedral angles between the dimethylphenyl plane *A* (C1–C6), the cyclobutane plane *B* (C9–C12), and the thiazole plane *C* (S/N1/C14–C16) are 32.31(24)° (*A*/*B*), 65.82(12)° (*A*/*C*), and 44.12 (17)° (*B*/*C*).

In the thiazole ring, the S1–C15 and S1–C16 bond lengths (Table 1) are shorter than the accepted value for an S–C(sp^2) single bond of 1.76 Å, resulting from the electron conjugation of S1 with C15 and C16 atoms [28]. The N2–C16 bond distance (1.343(4) Å) is shorter than a single bond [29] but longer than that of the double N1–C16 bond (1.316(4) Å) [30, 31], which suggests the existence of delocalized double bonds in the thiazole and amine moieties.

The steric interaction between the substituent groups on the cyclobutane ring means that this ring deviates significantly from planarity. In the cyclobutane ring, the C10/C11/C12 plane makes a dihedral angle of 28.44(45)° with the C12/C9/C10 plane. A survey of the geometry of cyclobutanes shows the average pucker to be 29.03(13)° [32], 28.16(3)° [33], and 29.55(2)° [34] in acyclic substituted cyclobutane rings, and the present value is in agreement with the previous reports.

The molecules are linked by the N–H…N intermolecular hydrogen bond (Table 2). The amine N2 atom in the molecule at (*x*, *y*, *z*) acts as a hydrogen bond donor, *via* the H2a hydrogen atom, to the thiazole N1 atom in the molecule at (–*x*, 1–*y*, –*z*), thus generating by translation an $R_2^2(8)$ dimer running nearly parallel to the [0 $\bar{1}$ 1] direction (Fig. 2). Apart from these hydrogen bonds, there are π…π interactions which stabilize the titled compound.

TABLE 1. Selected Theoretical and Experimental Geometric Parameters in the Titled Compound

Parameter	Experimental	B3LYP 6-31G(*d*)	Parameter	Experimental	B3LYP 6-31G(*d*)
		Bond lengths, Å			
S–C15	1.718(4)	1.752	N2–C17	1.438(4)	1.451
S–C16	1.733(4)	1.774	C14–C15	1.344(5)	1.363
N1–C14	1.387(4)	1.387	C9–C13	1.542(5)	1.541
N1–C16	1.316(4)	1.304	RMSE*		0.023
N2–C16	1.343(4)	1.369	Max. difference*		0.041
	Bond angles, deg			Dihedral angles, deg	
C15–S–C16	88.7(2)	87.89	S–C16–N2–C17	–1.5(5)	19.11
S–C16–N1	114.7(3)	114.89	N1–C16–N2–C17	179.5(4)	–162.91
N1–C16–N2	123.2(4)	123.66	C11–C14–N1–C16	–179.4(3)	179.97
C14–N1–C16	110.3(3)	111.05	C10–C11–C14–N1	66.0(5)	69.61
C11–C14–N1	116.5(4)	117.70	C12–C11–C14–C15	–9.2(6)	–3.78
C11–C14–C15	128.5(4)	126.57	C2–C1–C9–C12	33.1(5)	31.90
C16–N2–C17	122.5(4)	122.42	C6–C1–C9–C10	–49.4(5)	–48.90
RMSE*		0.97			
Max. difference*		1.93			

* RMSE and maximum differences between the bond lengths and the bond angles computed by the theoretical method and those obtained from X-ray diffraction.

TABLE 2. Hydrogen Bond Geometries in the Crystal Structure (Å, deg) (symmetry code: –*x*, 1–*y*, –*z*.)

D—H…A	D—H	H…A	D…A	D—H…A
N2—H2a…N1	0.86	2.09	2.931(4)	166

Optimized structure. The molecular structure of the titled compound ($C_{17}H_{22}N_2S$) in the ground state (*in vacuo*) is optimized using the B3LYP/6-31G(*d*) method. As seen from Table 1, most of the calculated bond lengths and bond angles are slightly different from the experimental ones. We noted that the experimental results belonged to the solid phase and theoretical calculations belonged to the gas phase. In the solid state, the experimental results are related to molecular packing, but in the gas phase, the isolated molecules are considered in the theoretical calculations. The biggest difference between the experimental and predicted bond lengths is found for the S–C16 bond with the difference being 0.041 Å for the B3LYP method, whereas the biggest difference for the bond angles is found to be 1.93° for C11–C14–C15. Using the root mean square error (RMSE) for evaluation, RMSE values of bond lengths and angles are 0.023 Å and 0.97°, respectively. In

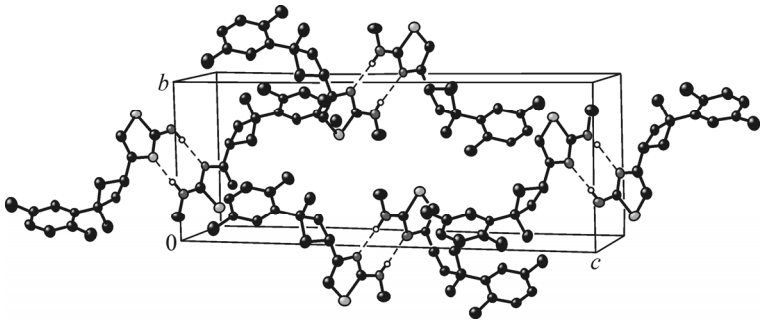

Fig. 2. Diagram showing the N—H…N intermolecular hydrogen bonds in the titled compound. Only H atoms involved in the hydrogen bonding interactions are shown. (Symmetry code: –*x*, 1–*y*, –*z*.)

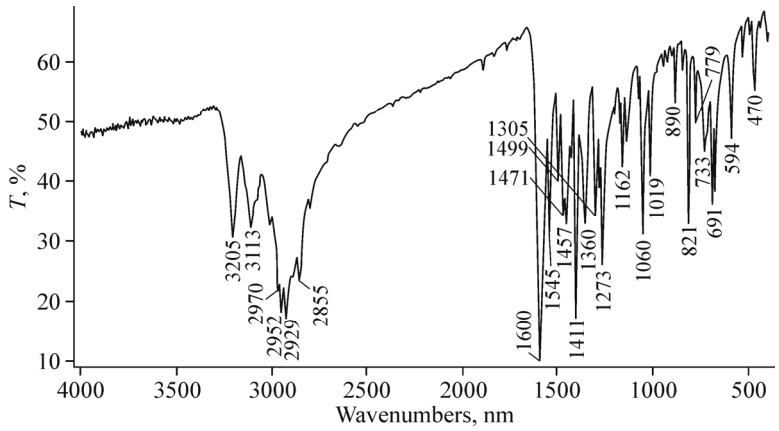

Fig. 3. FT-IR spectrum of the titled compound.

addition, the dihedral angles between the optimized counterparts of the titled compound are calculated as 38.72° (*A*/*B*), 68.61° (*A*/*C*), 46.61° (*B*/*C*) for DFT/6-31G(*d*). Despite the differences observed, the calculated geometric parameters are, in general, in good agreement with the X-ray structure.

IR spectroscopy. The FT-IR spectrum was obtained in KBr discs using a Mattson 1000 FT-IR spectrometer and is shown in Fig. 3. Harmonic vibrational frequencies of the titled compound were calculated by the DFT method with 6-31G(*d*) and 6-31++G(*d*,*p*) basis sets, and the obtained frequencies were scaled by 0.9772 [22] and 0.9537 [23]. Using the Gauss-View molecular visualization program [21], the vibrational band assignments have been made. The calculated and experimental frequencies show differences. Two factors may be responsible for the discrepancies between the experimental and computed spectra of the investigated molecule. The first reason is that the experimental spectrum has been recorded for the compound in the solid state, while the computed spectra correspond to an isolated molecule in the gas phase. The second reason is the fact that the experimental values correspond to anharmonic vibrations, while the calculated values are harmonic vibrations [29]. In order to facilitate the assignment of the observed peaks we have analyzed the vibrational frequencies and compared our calculation of the titled compound with their experimental data. The results and shown in Table 3.

The experimental N–H stretching mode was observed at 3205 cm^{-1}, which has been calculated at 3517 cm^{-1} at B3LYP/6-31G(*d*) and 3454 cm^{-1} at B3LYP/6-31++G(*d*,*p*) levels. The experimental peak is in good agreement in the NH region [35, 36] As can be easily seen, the experimental value of the N–H stretching mode is smaller than the calculated frequencies because the titled compound with the amine group is involved in the hydrogen bonding. The aromatic structure shows the presence of C–H stretching vibrations in the region 2900-3150 cm^{-1}, which is the characteristic region for the ready identification of the C–H stretching vibrations [37]. In the present study, the experimental C–H stretching vibration of the titled compound is observed at 3113 cm^{-1}, while it has been calculated at 3114 cm^{-1} by B3LYP6-31G(*d*) and 3035 cm^{-1} by B3LYP/6-31++G(*d*,*p*). The asymmetric CH_2 stretching vibrations are generally observed in the region 3100-3000 cm^{-1}, while the symmetric stretch appears between 3000 cm^{-1} and 2900 cm^{-1} [38, 39-41]. The symmetric stretching is observed as a medium intense shoulder in the IR spectrum at 2952 cm^{-1}. The *ab initio* calculation gives the frequency of these bands at 3060 cm^{-1} and 2980 cm^{-1} for the CH_2 asymmetric stretch and 2994 cm^{-1} and 2913 cm^{-1} for the CH_2 symmetric stretch at the B3LYP/6-31G(*d*) and B3LYP/6-31++G(*d*,*p*) levels, respectively. The thiazole (C=N) bond stretching vibration was experimentally observed to be 1600 cm^{-1}, while that was calculated at 1590 cm^{-1} at the B3LYP/6-31G(*d*) and B3LYP/6-31++G(*d*,*p*) levels, respectively. The benzene ring modes predominantly involve C=C bonds and the vibrational frequency is associated with the C=C stretching modes of the carbon skeleton [42]. The C=C stretching modes predicted at 1545-1457 cm^{-1} are in good agreement with the calculated values at 1547 cm^{-1} and 1498 cm^{-1}.

The other calculated vibrational frequencies can be seen in Table 3. As can be seen from Table 3, there is also good agreement between the experimental and theoretical vibrational data for the others.

Molecular electrostatic potential. The molecular electrostatic potential (MEP) is related to the electron density and is a very useful descriptor in understanding the sites of the electrophilic attack and nucleophilic reactions as well as hydrogen

TABLE 3. Comparison of the Observed and Calculated Vibrational Spectra of the Titled Compound

Assignments	Experimental	B3LYP6-31G(*d*)	B3LYP6-31G++(*d*,*p*)	Assignments	Experimental	B3LYP6-31G(*d*)	B3LYP6-31G++(*d*,*p*)
ν N–H	3205	3517	3454	ν C=C (aromatic)	1457	–	–
ν_s C–H (aromatic)	3113	3114	3035	γ CH (aromatic)	1411	1512	1463
ν_{as} C–H (aromatic)		3103	3026	β CH_3		–	1437
ν_{as} C–H (aromatic)		3096	3017	β CH_3		–	1390
ν_{as} C–H (aromatic)		3075	2994	α CH_3	1360	1480	–
ν_{as} C–H_2		3060	2980	γ NH	1305	–	1365
ν_{as} C–H_3		3050	2970	γ NH	1273	1411	–
ν_{as} C–H_3 + ν_{as} C–H_2	2970	3049	2969	γ CH	1162	1379	1335
ν_{as} C–H_3 + ν_{as} C–H_2		3047	2966	ν C–N	1060	1303	1264
ν_{as} C–H_3		3040	2958	ν C–C (aromatic) + ω CH_2		1301	1257
ν_{as} C–H_3		3022	2944	γ CH	1019	1278	1237
ν_{as} C–H_3		3019	2936	β CH_3	–	1174	1136
ν_s C–H_2		3005	2925	δ CH_3	890	1132	1094
ν_s C–H_2	2952	2994	2913	ν C–N (aliphatic)	821	1037	1005
ν C–H		2990	–	ν C–N (aliphatic)	779	–	–
ν_s C–H_3		2983	2904	ω CH (aromatic)	733	808	785
ν_s C–H_3		2976	2894	ν C–S (thiazole)	691	767	745
ν_s C–H_3	2929	2970	2890	β CH (thiazole)		683	655
ν_s C–H_3	2855	2945	2866	β CH (thiazole) + β NH		605	578
ν C=N (thiazole)	1600	1590	1536	β CH (thiazole)	594	573	563
ν C=C (thiazole)	1545	1547	1498	β NH + β CH_2	470	440	–
ν C=C (aromatic)	1499	–	–	β NH		424	396
ν C=C (aromatic)	1471	–	–				

Vibrational modes: ν, stretching; β, bending; α, scissoring; γ, rocking; ω, wagging; δ, twisting; θ, ring breathing; s, symmetric; as, asymmetric.

bonding interactions [43-45]. The electrostatic potential $V(r)$ is also well suited for analyzing processes based on the "recognition" of one molecule by another, such as in drug–receptor, and enzyme–substrate interactions, because it is through their potentials that the two species first "see" each other [46, 47]. Being a real physical property, $V(r)$ can be determined experimentally by diffraction or computational methods [48].

MEP was calculated by the B3LYP/6-31G(*d*) method. The red and blue regions of MEP represent the negative and positive potentials, respectively. As can be seen in Fig. 4, this molecule has one possible site of the electrophilic attack. The

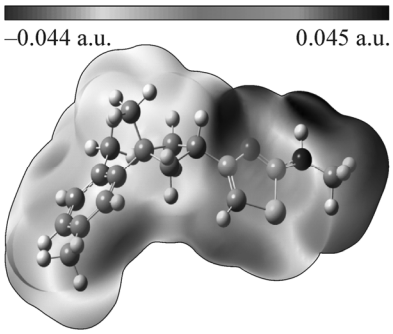

Fig. 4. Molecular electrostatic potential (MEP) map calculated at the B3LYP/6-31G(*d*) level.

TABLE 4. Theoretical and Experimental ^{13}C and ^{1}H Isotropic Chemical Shifts (with respect to TMS; all values in ppm) for the Titled Compound

Atom	Experimental, ppm $CDCl_3$	Calculated chemical shifts, ppm		Atom	Experimental, ppm $CDCl_3$	Calculated chemical shifts, ppm	
		B3LYP/6-31G(*d*)	B3LYP/6-311G+(2*d*,*p*)			B3LYP/6-31G(*d*)	B3LYP/6-311G+(2*d*,*p*)
C1	149.12	142.62	157.65	C16	171.18	164.29	178.68
C2	126.20	120.40	131.78	C17	32.01	31.02	32.52
C3	134.99	128.74	142.09	H2	6.95	6.81	7.20
C4	126.32	120.16	130.40	H2a	5.83	3.73	4.36
C5	130.86	124.92	135.65	H4	6.84	6.73	7.12
C6	131.30	126.14	138.70	H5	6.90	6.80	7.17
C7	20.88	21.72	23.30	H7*	2.23	2.16	2.31
C8	19.40	21.89	22.46	H8*	2.30	2.07	2.25
C9	39.59	42.57	46.12	H10*	2.45-2.58	2.40	2.30
C10	41.02	43.03	45.68	H11	3.55	3.57	3.51
C11	31.18	32.76	35.85	H12*	2.45-2.58	2.49	2.47
C12	41.02	37.72	40.72	H13*	1.53	1.47	1.41
C13	27.38	27.52	28.38	H15	6.08	5.59	6.14
C14	156.99	149.02	165.34	H17*	2.89	2.69	2.81
C15	99.05	101.78	106.87				

* Average.

negative region is localized on the unprotonated N1 nitrogen atom of the thiazole ring with a minimum value of –0.044 a.u. However, maximum positive regions are localized on the N2 nitrogen atom of the amine group and the hydrogen atom of the methyl group, which can be considered as possible sites for the nucleophilic attack with maximum values of 0.045 a.u. and 0.034 a.u., respectively. According to these calculated results, the MEP map shows that the negative potential site is on the electronegative atom while the positive potential sites are around the hydrogen atoms of the methyl-amine group. These sites give information about the region where the compound can have intermolecular interactions.

^{1}H and ^{13}C NMR spectra. DFT methods treat the electronic energy as a function of the electron density of all electrons simultaneously and thus include the electron correlation effect [49]. GIAO ^{1}H and ^{13}C chemical shift values (with respect to TMS) calculated by the B3LYP/6-31G(*d*) and B3LYP/6-311+G(2*d*,*p*) methods were compared to the experimental ^{1}H and ^{13}C chemical shift values. The ^{1}H and ^{13}C chemical shifts were measured in $CDCl_3$. The results are given in Table 4.

Since the experimental ^{1}H chemical shift values were not available for an individual hydrogen atom, we have presented the average values for CH_2 and CH_3 hydrogen atoms. The singlet observed at 6.08 ppm is assigned to H15 (C15) atoms and it was calculated at 5.59 ppm and 6.14 ppm at the B3LYP/6-31G(*d*) and B3LYP/6-311+G(2*d*,*p*) levels, respectively. The cyclobutane $–CH_2–$ signals were observed at 2.45-2.58 ppm. The aromatic H atoms were observed at 6.84-6.95 (H2, H4, H5) ppm. The N–H hydrogen atom in the amine group appears at 5.83 ppm. In the formation of the intermolecular hydrogen bond the amine group causes a deviation of the chemical shift value and therefore the H atom (H2a) contributes to the downfield resonance. ^{13}C NMR spectra of the thiazole compound show the signals at 99.05-171.18 ppm due to C atoms. These signals have been calculated as 101.78-164.29 ppm and 106.87-178.68 ppm at the B3LYP/6-31G(*d*) and B3LYP/6-311+G(2*d*,*p*) levels. Table 4 shows the other calculated chemical shift values. As can be seen from Table 5, calculated with a larger basis set, ^{1}H chemical shift values of the titled compound are generally in better agreement with the experimental ^{1}H shift data.

Frontier molecular orbital analysis. The frontier molecular orbitals play an important role in the electric and optical properties as well as in UV-Vis spectra and chemical reactions [50]. The distributions and energy levels of the HOMO-1, HOMO, LUMO, and LUMO+1 orbitals computed at the B3LYP/6-31G(*d*) level for the titled compound are shown in Fig. 5.

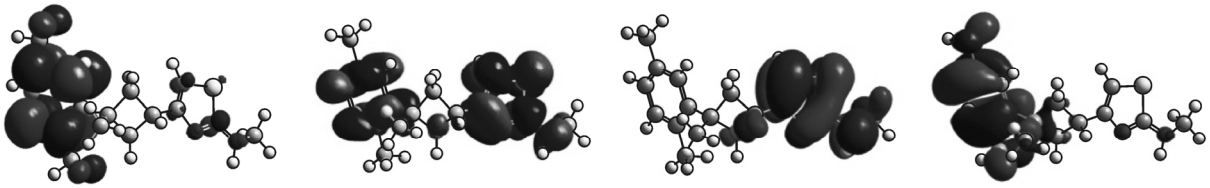

Fig. 5. Plots of the frontier orbitals of the titled compound.

As seen from Fig. 5, the HOMOs are mainly localized on methylthiazol-2-amine and partially on the cyclobutane fragment. However, HOMO-1 is localized on the dimethylphenyl and cyclobutane rings of the titled molecule and partially on thiazol and amine N atoms. The LUMOs are localized on the whole structure, except methyl groups. LUMO+1 is localized on the dimethylphenyl ring and par tially on the methylthiazol-2-amine fragment. HOMO-1 and HOMOs are π-bonding type orbitals. In all cases, LUMO and LUMO+1s are π*-antibonding type orbitals. The energy separation between the HOMO and LUMO is 5.549 eV, and this value indicates the energy gap of the titled compound.

Nonlinear optical effects. Nonlinear optical (NLO) effects arise from the interactions of electromagnetic fields in various media producing new fields altered in the phase, frequency, amplitude, or other propagation characteristics from the incident field [51]. NLO is at the forefront of the current research because of its importance in providing the key functions of the frequency shifting, optical modulation, optical switching, optical logic, and optical memory for the emerging technologies in areas such as telecommunications, signal processing, and optical interconnections [52-55].

The nonlinear optical response of an isolated molecule in an electric field $E_i(\omega)$ can be presented as a Taylor series expansion of the total dipole moment μ_{tot} induced by the field

$$\mu_{tot} = \mu_0 + \alpha_{ij}E_j + \beta_{ijk}E_jE_k + \dots , \quad (2)$$

where α_{ij} is the linear polarizability, μ_0 is the permanent dipole moment, and β_{ijk} are the first hyperpolarizability tensor components. The isotropic (or average) linear polarizability is defined as [56]

$$\alpha_{tot} = \frac{\alpha_{xx} + \alpha_{yy} + \alpha_{zz}}{3} . \quad (3)$$

The first hyperpolarizability is a third rank tensor that can be described by a 3×3×3 matrix. The 27 components of the 3D matrix can be reduced to 10 components due to the Kleinman symmetry [57] ($\beta_{xyy} = \beta_{yxy} = \beta_{yyx}$, $\beta_{yyz} = \beta_{yzy} = \beta_{zyy}$; … likewise other permutations also take the same value). The output from Gaussian 03 provides 10 components of this matrix as β_{xxx}, β_{xxy}, β_{xyy}, β_{yyy}, β_{xxz}, β_{xyz}, β_{yyz}, β_{xzz}, β_{yzz}, β_{zzz}, respectively. The components of the first hyperpolarizability can be calculated using the following equation [56]:

$$\beta_i = \beta_{iii} + \frac{1}{3}\sum_{i \neq j}(\beta_{ijj} + \beta_{jij} + \beta_{jji}). \quad (4)$$

Using the *x*, *y*, and *z* components of β, the magnitude of the first hyperpolarizability tensor can be calculated by

$$\beta_{tot} = \sqrt{(\beta_x^2 + \beta_y^2 + \beta_z^2)} . \quad (5)$$

The complete equation for calculating the β magnitude from the Gaussian 03W output is given as follows:

$$\beta_{tot} = \sqrt{(\beta_{xxx} + \beta_{xyy} + \beta_{xzz})^2 + (\beta_{yyy} + \beta_{yzz} + \beta_{yxx})^2 + (\beta_{zzz} + \beta_{zxx} + \beta_{zyy})^2} . \quad (6)$$

The calculations of the total molecular dipole moment (μ), linear polarizability (α), and first-order hyperpolarizability (β) from the Gaussian output have been explained in detail previously [57], and DFT has been extensively used as an effective method to investigate the organic NLO materials [58-63]. To investigate the effects of basis sets on the NLO properties of compound I, μ_{tot}, α_{tot}, and β_{tot} were calculated by the B3LYP method with the 6-31G(*d*), 6-31+G(*d*,*p*), and 6-31++G(*d*,*p*) basis sets and are listed in Table 5.

TABLE 5. HOMO-LUMO Gap, Total Dipole Moment (μ), Polarizability (α), and First Hyperpolarizability (β) of Titled Compound **I**

Basis set	Gap, eV	μ, D	α, Å^3	β, (cm^5/esu)×10^{-30}
6-31G(*d*)	5.55	0.70	30.32	2.02
6-31+G(*d*)	5.22	0.81	34.67	4.02
6-31++G(*d*)	5.14	0.81	34.85	3.78

From Table 5, we see that the calculated values of μ_{tot}, α_{tot}, and β_{tot} slightly depend on the size of basis sets. The obtained μ_{tot}, α_{tot}, values with the 6-31G(*d*) basis set are smaller than those obtained with the other basis sets. However, the β_{tot} value obtained by the medium size basis set is bigger than that given by a large basis set.

Urea is one of the prototypical molecules used in the study of the NLO properties of molecular systems because there are no experimental values for the titled compound. Therefore, it was used frequently as a threshold value for comparative purposes. It can be seen from Table 5 that the calculated α_{tot} and β_{tot} values for the titled molecule are greater than those of urea (α_{tot} and β_{tot} of urea are 3.831 Å^3 and 0.3728×10^{-30} cm^5/esu obtained by the B3LYP/6-31G(*d*) metho*d*). These results indicate that the titled compound can be a potential candidate of the second order NLO material.

To understand this phenomenon in the context of the molecular orbital theory, we examined the molecular HOMOs and LUMOs of the titled molecule. The calculated energy gaps are also listed in Table 5. The HOMO-LUMO energy gaps were calculated as 5.14-5.55 eV for the titled molecule. As can be seen from the β_{tot} values for the titled compound, there is an inverse relationship between the first hyperpolarizability and the HOMO-LUMO gap, allowing the molecular orbitals to overlap to have a proper electronic communication conjugation, which is a marker of the intramolecular charge transfer from the electron donating group to the electron accepting group through the π conjugation system [64-66].

CONCLUSIONS

In this work, the compound has been characterized by ^{1}H and ^{13}C NMR, X-ray diffraction, and FT-IR techniques. The crystal structure is stabilized by N–H···N hydrogen bond interactions. Density functional calculations have been performed for **I**, and the calculated results show that B3LYP/6-31G(*d*), B3LYP/6-31++G(*d*,*p*), and B3LYP/6-311+G(2*d*,*p*) levels can reproduce well the crystal structure, theoretical vibrational frequencies, and chemical shift values of **I**. The MEP map shows that the negative potential sites are on electronegative atoms, whereas the positive potential sites are around the hydrogen atoms. The predicted nonlinear optical (NLO) properties of the titled compound are greater than those of urea. The titled compound is a good candidate as the second-order NLO material. As a result, all of these calculations will provide helpful information for further studies on the titled compound.

Crystallographic data for the structural analysis have been deposited with the Cambridge Crystallographic Data Centre, CCDC No 874368. Copy of this information may be obtained free of charge from the Director, CCDC, 12 Union Road, Cambridge CB2 1EZ, UK (fax: +44-1223-336033; e-mail: deposit@ccdc.cam.ac.uk or www: http://www.ccdc.cam.ac.uk).

REFERENCES

1. H. Zollinger, *Colour Chemistry Syntheses Properties and Applications of Organic Dyes and Pigments*, 2nd ed., VCH, Weinheim (1991**)**.
2. P. J. Islip, M. D. Closier, and M. C. Neville, *J. Med. Chem.*, **17,** No. 2, 207-209 (1974).
3. K. Brown, D. P. Cater, J. F. Cavalla, D. Green, R. A. Newberry, and A. B. Wilson, *J. Med. Chem.,* **17,** No. 11, 1177-1181 (1974).
4. L. Coghi, A. M. M. Lanfredi, and A. Tripicchio, *J. Chem. Soc., Perkin Trans. 2*, 1808-1810 (1976).

5. V. A. Saprykina, V. I. Vinogradova, R. F. Ambartsumova, T. F. Ibragimov, and Kh. M. Shakhidoyatov, *Chem. Nat. Compd.*, **42**, 4470-4472 (2006).
6. J. D. Hadjipavlou-Litina and A. Geronikaki, *Arzneim.-Forsch./ Drug Res.*, **46**, 805-808 (1996).
7. A. Cukurovali, I. Yilmaz, S. Gur, and C. Kazaz, *Eur. J. Med. Chem.*, **41**, 201-207 (2006).
8. F. D. Proft and P. Geerlings, *Chem. Rev.*, **101**, 1451-1464 (2001).
9. G. Fitzgerald and J. Andzelm, *J. Phys. Chem.*, **95**, 10531-10534 (1991).
10. T. Ziegler, *Pure Appl. Chem.*, **63**, 873-878 (1991).
11. J. Andzelm and E. Wimmer, *J. Chem. Phys.*, **96**, 1280-1303 (1992).
12. G. E. Scuseria, *J. Chem. Phys.*, **97**, 7528-7530 (1992).
13. R. M. Dickson and A. D. Becke, *J. Chem. Phys.*, **99**, 3898-3905 (1993).
14. B. G. Johnson, P. M. W. Gill, and J. A. Pople, *J. Chem. Phys.*, **98**, 5612-5626 (1993).
15. N. Oliphant and R. J. Bartlett, *J. Chem. Phys.*, **100**, 6550-6556 (1994).
16. M. A. Akhmedov, I. K. Sardarov, I. M. Akhmedov, R. R. Kostikov, A. V. Kisin, and N. M. Babaev, *Zh. Org. Khim.*, **27**, 1434 (1991).
17. G. M. Sheldrick, *SHELXS-97 & SHELXL-97*, University of Göttingen, Germany (1997).
18. H. B. Schlegel, *J. Comput. Chem.*, **3**, 214-218 (1982).
19. C. Peng, P. Y. Ayala, H. B. Schlegel, and M. J. Frisch, *J. Comput. Chem*., **17**, 49-56 (1996).
20. M. J. Frisch, G. W. Trucks, H. B. Schlegel, et al., *GAUSSIAN-03*, *Revision E.01*, Gaussian Inc., Wallingford, CT (2004).
21. A. Frisch, R. I. I. Dennington, T. Keith, J. Millam, A. B. Nielsen, A. J. Holder, and J. Hiscocks, *GaussView Reference, Version 4.0*, Gaussian Inc., Pittsburgh (2007).
22. A. P. Scott and L. Radom, *J. Phys. Chem.*, **100**, 16502-16513 (1996).
23. Y. Zhao and D. G. Truhlar, *J. Phys. Chem. A*, **108**, 6908-6918 (2004).
24. R. Ditchfield, *J. Chem. Phys.*, **56,** No. 11, 5688-5691 (1972).
25. K. Wolinski, J. F. Hinton, and P. Pulay, *J. Am. Chem. Soc.*, **112,** No. 23, 8251-8260 (1990).
26. P. Politzer and J. S. Murray, *Theor. Chem. Acc.*, **108**, 134-142 (2002).
27. L. J. Farrugia, *J. Appl. Crystallogr.,* **30**, 565/566 (1997).
28. F. H. Allen, *Acta Crystallogr.*, **B40**, 64-72 (1984).
29. I. Kowalczyk, E. Bartoszak-Adamska, M. Jasko´lski, Z. Dega-Szafran, and M. Szafran, *J. Mol. Struct.*, **976**, 119-128 (2010).
30. G. Liu, L. Liu, D. Jia, and K. Yu, *J. Chem. Crystallogr.*, **35**, 497 (2005).
31. Q. Ma, L.-P. Lu, and M.-L. Zhu, *Acta Crystallogr.*, **E64**, o2026 (2008).
32. Ç. Yüksektepe, H. Saraçoğlu, M. Koca, A. Cukurovali, and N. Çalışkan, *Acta Crystallogr*., **C60**, o509/o510 (2004).
33. Ç. Yüksektepe, S. Soylu, H. Saraçoğlu, N. Çalışkan, A. Cukurovali, I Yılmaz, and C. Kazaz, *Acta Crystallogr*., **E61**, o2384-o2386 (2005).
34. M. S. Soylu, N. Çalışkan, A. Cukurovali, I. Yılmaz, and O. Büyükgüngör, *Acta Crystallogr*., **C61**, o725-o727 (2005).
35. N. P. G. Roeges, *A Guide to the Complete Interpretation of Infrared Spectra of Organic Structures,* Wiley, Chichester (1994), ch. 9.
36. G. Herzberg, *Molecular Spectra and Molecular Structure,* vol. 2, Van Nostrand, New York (1945), chap. 3, sect. 3.
37. A. Teimouri, M. Emami, A. N. Chermahini, and H. A. Dabbagh, *Spectrochim. Acta*, **71A**, 1749-1755 (2009).
38. I. Hubert Joe, G. Aruldhas, S. Anbukumar, and. P. Ramasamy, *Cryst. Res. Technol.*, **29**, 685-692 (1994).
39. G. Litvinov, *Proc. Int. Conf. Raman Spectrosc., 13th*, Wurzburg, Germany (1992).
40. K. Furic, V. Mohacek, M. Bonifacic, and I. Stefanic, *J. Mol. Struct.* **267**, 39-44 (1992).
41. G. Lan, H. Wang, and J. Zheng, *Spectrochim. Acta,* **46A**, 1211-1216 (1990).
42. A. Teimouri, A. N. Chermahini, K. Taban, and H. A. Dabbagh, *Spectrochim Acta*, **72A**, 369-377 (2009).

43. E. Scrocco and J. Tomasi, *Adv. Quant. Chem.*, 11, 115-193 (1978).
44. F. J. Luque, J. M. Lopez, and M. Orozco, *Theor. Chem. Acc*., **103**, 343-345 (2000).
45. N. Okulik and A. H. Jubert, *Internet Electron J. Mol. Des***.**, **4**, 17-30 (2005).
46. P. Politzer, P. R. Laurence, and K. Jayasuriya, *Environ. Health Perspect.*, **61**, 191-202 (1985).
47. E. Scrocco and J. Tomasi, *Top. Curr. Chem.*, **7**, 95-170 (1973).
48. P. Politzer and D. G. Truhlar, *Chemical Applications of Atomic and Molecular Electrostatic Potentials*, Plenum Press, New York (1981).
49. S. Demir, M. Dinçer, E. Korkusuz, and İ. Yıldırım, *J. Mol. Struct.*, **980**, 1-6 (2010).
50. I. Fleming, *Frontier Orbitals and Organic Chemical Reactions*, John Wiley, London (1976).
51. Y. X. Sun, Q. L. Hao, W. X. Wei, Z. X. Yu, L. D. Lu, X. Wang, Y. S. Wang, *J. Mol. Struct.: THEOCHEM*, **904**, 74-82 (2009).
52. C. Andraud, T. Brotin, C. Garcia, F. Pelle, P. Goldner, B. Bigot, and A. Collet, *J. Am. Chem. Soc*., **116**, 2094-2102 (1994).
53. V. M. Geskin, C. Lambert, and J. L. Bredas, *J. Am. Chem. Soc*., **125**, 15651-15658 (2003).
54. M. Nakano, H. Fujita, M. Takahata, and K. Yamaguchi, *J. Am. Chem. Soc*., **124**, 9648-9655 (2002).
55. D. Sajan, H. Joe, V. S. Jayakumar, and J. Zaleski, *J. Mol. Struct*., **785**, 43-53 (2006).
56. R. Zhang, B. Du, G. Sun, and Y. X. Sun, *Spectrochim. Acta*, **75A**, 1115-1124 (2010).
57. D. A. Kleinman, *Phys. Rev*., **126**, 1977-1979 (1962).
58. K. S. Thanthiriwatte and K. M. Nalin de Silva, *J. Mol. Struct.: THEOCHEM*, **617**, 169-175 (2002).
59. Y. X. Sun, Q. L. Hao, Z. X. Yu, W. X. Wei, L. D. Lu, and X. Wang, *Mol. Phys.*, **107**, 223-235 (2009).
60. A. B. Ahmed, H. Feki, Y. Abid, H. Boughzala, C. Minot, and A. Mlayah, *J. Mol. Struct.*, **920**, 1-7 (2009).
61. J. P. Abraham, D. Sajan, V. Shettigar, S. M. Dharmaprakash, I. Nemec, I. H. Joe, and V. S. Jayakumar, *J. Mol. Struct.*, **917**, 27-36 (2009).
62. S. G. Sagdinc and A. Esme, *Spectrochim. Acta*, **75A**, 1370-1376 (2010).
63. A. B. Ahmed, H. Feki, Y. Abid, H. Boughzala, and C. Minot, *Spectrochim. Acta*, **75A**, 293-298 (2010).
64. M. C. Ruiz Delgado, V. Hernandez, J. Casado, J. T. Lopez Navarre, J. M. Raimundo, P. Blanchard, and J. Roncali, *J. Mol. Struct.: THEOCHEM*, **709**, 187-193 (2004).
65. M. C. Ruiz Delgado, V. Hernandez, J. Casado, J. T. Lopez Navarre, J. M. Raimundo, P. Blanchard, and J. Roncali, *J. Mol. Struct.*, **651-653**, 151-158 (2003).
66. J. P. Abraham, D. Sajan, V. Shettigar, S. M. Dharmaprakash, I. Nemec, I. Hubert Joe, and V. S. Jayakumar, *J. Mol. Struct.*, **917**, 27-36 (2009).